TR(BR)-7/97-98

Overland Flow Modelling for Urban Catchment Considering Random Roughness Coefficients and Irregular Land Surface

आपो हि ष्ठा मयोभुवः

NATIONAL INSTITUTE OF HYDROLOGY
JAL VIGYAN BHAWAN
ROORKEE - 247 667 (U.P.) INDIA

1997-98

CONTENTS

LIST OF FIGURES i
LIST OF TABLES ii
ABSTRACT iii

1. INTRODUCTION 1
    1.1 General 1
    1.2 Literature Review 2

2. GOVERNING EQUATIONS 5
    2.1 Surface Flow Equations 5
    2.2 Subsurface Flow Equations 7

3. NUMERICAL METHOD 10
    3.1 Surface Flow 10
        3.1.1 Finite-Volume Scheme 11
        3.1.2 Initial Conditions 17
        3.1.3 Boundary Conditions 17
        3.1.4 Numerical Stability 20
    3.2 subsurface Flow 20
        3.2.1 Implicit Finite-Difference Scheme 21
        3.2.2 Boundary Conditions 24
    3.3 Surface and subsurface Flow Interaction 25

4. RESULTS AND DISCUSSION 27
    4.1 Validation of the model 27
        4.1.1 Surface Flow 27
        4.1.2 Subsurface Flow 30
    4.2 Simulation of Hypothetical urban catchment 30

5. CONCLUSION 35

REFERENCES

APPENDIX I. Notation

LIST OF FIGURES

Fig. 1: Definition sketch for the urban catchment with impervious area. 4

Fig. 2: Finite-volume grid for two-dimensional domain. . 12

Fig. 3: Two-dimensional cells for any arbitrary shape of flow domain (Non-orthogonal cell). 12

Fig. 4: Normal vectors at the cell faces in a cell of two-dimensional finite-volume grid. 13

Fig. 5: Implementation of boundary conditions
(a) Solid wall (b) Corner Inflow and (c) Line Inflow. 18

Fig. 6a: Finite-Difference Grid for Subsurface Flow.

6b: Definition Sketch of Pressure Head type Boundary for Subsurface Flow. 21

Fig. 7: Comparison of outflow hydrograph from surface flow model with uniform surface roughness. 29

Fig. 8: Comparison of outflow hydrograph from surface flow model with variable surface roughness. 29

Fig. 9: Comparison of moisture content profile for subsurface flow model. 31

Fig. 10: Comparison of Infiltration rate with earlier results. 31

Fig. 11: Comparison of Cumulative Infiltration with earlier results. 32

Fig. 12: Effect of urbanization on runoff hydrograph. . . 34

LIST OF TABLES

Table 1: Spatial Distribution of Surface Roughness 28
Table 2: Computational Parameters for Subsurface. 30
Table 3: Hydraulic Properties of the Soil. 33

ABSTRACT

Urbanization is defined as the concentration of people in urban settlements and the process of change in land use occupancy resulting from the conversion of rural land into urban, suburban and industrial communities. The world growth of urbanization over the years is of logarithmic pattern. In more developed countries, about 75% of the population is concentrated in urban areas and in developing countries, like India, the rate of urban growth is very high. The rapid process of urbanization in India is a challenge for administrators, planners and research workers. This rapid process of urbanisation is causing heavy demand for water necessitating increase in the construction of water supply and drainage facilities. With increase in impervious area due to urbanization there has been increase in runoff peak and runoff volume and decrease in time to peak. Design of drainage facilities, which do not account for this increased runoff volume, are inadequate and thus needs to develop an overland flow model for urban catchment in order to estimate the exact runoff and time to peak.

In this study, a two-dimensional overland flow model has been developed considering random roughness coefficients and irregular land surface for the analysis of surface flow component. One-dimensional Richards equation for subsurface flow component has been used for calculating the infiltration from pervious area. The surface and subsurface flow models are linked explicitly at the ground surface through the processes of infiltration. These two models have been validated separately for surface flow and subsurface flow using earlier results. Present model is used to simulate a hypothetical urban catchment.

1. INTRODUCTION

1.1 General

Urbanization is defined as the concentration of people in urban settlements and the process of change in land use occupancy resulting from the conversion of rural lands into urban, suburban and industrial communities (Davis, 1965 and Savani and Kammerer, 1961). Urbanisation includes the transformation of a rural set-up to an urban set-up, development of a sub-urban area to an urban area and rural-urban migration. The urban areas have developed in response to human social and economic needs. The important causes of urbanization are : advances in science and technology, industrialization, advances in agriculture, better scope of employment, service oriented business, better education facilities, medical facilities and improvement in transportation. The forces of urbanization are a product of man's genius, of his continuous quest for efficiency and of his need for the social and cultural milieu that an urban area can provide (Lazaro, 1990).

The world growth of urbanization over the years is of logarithmic pattern. In 1950 about one-third of the world population were lived in cities. In 35 years since 1950, the number of people living in cities almost tripled, increasing by 1249 millions (734 to 1983 million). In more developed countries, about 75 % of the population is concentrated in urban areas. On a world-wide scale, total population growth during this century has been accompanied by a continuous increase in the ratio of urban to rural dwellers (McPherson, 1974). The rate of urban growth is especially high in developing countries like India. In India urban population increased to about 46.2 % during 1971 to 1981. During this period urban population of India has gone up from 109 million in 1971 to 156 million in 1981. Number of towns in India with a population over 20000 increased from 536 in 1951 to 975 in 1971. By 1991 the urban population in India is estimated to go up to 216 million and by 2001 it is estimated to go upto about 320 million. Such trend are reflected in the growth

of metropolitan cities including 5 in India that are expected to have more than 10 by the year 2001.

The rapid process of urbanization in India is a challenge for administrators, planners and research workers. As urban areas continue to expand new sources of water are required to be found. This rapid process of urbanisation is causing heavy demand of water for domestic, industrial and recreational purposes with the consequent increase in the construction of water supply and drainage facilities. The higher demand of water results in higher urban discharge, because of increase in residential and commercial facilities such as building, pavements and parking lots, the built up or impervious areas in the urban area increases. There is a increase in runoff peak and runoff volume, decrease in time to peak, decrease in infiltration and reduce of base flow. Design of drainage facilities which do not account for this increased runoff volume are inadequate and may result in heavy damage and loss of property. Therefore, there is a need for the correct estimation of storm runoff and design of suitable drainage system. This motivates the researcher to develop a model for overland flow on urban catchment to estimate the exact runoff, time to peak and to check the adequacy of the existing drainage facilities.

In this report, two-dimensional overland flow model has been developed considering random roughness coefficients and irregular land surface for analysing surface flow. Infiltration has been calculated using the one-dimensional Richards equation for subsurface flow.

1.2 Literature Review

An extensive literature review on urban hydrological modelling and catchment research has been carried out for different developed and developing countries in the report SR-15. The study showed that almost in all the countries the authentic data on long term basis are not available, specially the discharge data through urban drains.

Storm water management model (SWMM) is a package of models linked together and divided into a number of blocks. It is a comprehensive model covering both quantity and quality aspects. It was developed by the US Environmental Protection Agency in the early 1970 and is being continuously updated. It has been extensively used in the USA to design sewer upgrading works particularly where these are required to control pollution. It can models all the major hydrological processes but as a results becomes very unwieldy to apply in Indian hydrological condition.

UNESCO, 1978 reported that design of urban drainage system in India is based on rational formula because of lack of adequate continuous records of precipitation and stream flow.

Ramaseshan, UNESCO 1983, has also reported that the urban hydrologic problems of India differ from those of developed countries in several important points such as lateral rather than vertical development, limited amounts of paved area, initial interaction between urban drainage and flood control, preference for open drains over closed ones, limited availability of continuous records of precipitation, stream flow and water quality, limited number of sewer connections and hence shifting of combined sewer, high cost of construction and modification and limited capacity of financial investment.

Chakraborti A. K. (1989) in his study of urban storm water runoff modelling in Rohini Delhi has reported that the urban drainage index adopted in his study in India is 3.5 cumec/sq. km with 35 mm/hr rainfall intensity with once in two years recurrence interval. Since the rate of urbanisation in Rohini is expected to increase from 55 % to 84 % , the urban drainage index needs to be modified according to 5.5 cumec/sq km.

In the present study, a overland flow model for urban catchment considering the random roughness and irregular boundaries has been presented. This model is based on the solution of the two-dimensional shallow water flow equations for the surface flow by a finite-volume technique. A finite-volume technique has the advantage of being applicable to irregular fields without the necessity of approximations at the boundaries as required by a finite-difference scheme. One-dimensional

Richards equation has been used for calculating the actual infiltration considering actual physical conditions through the pervious surface. The solution of Richards equation has been obtained using the implicit finite difference technique. Boundary conditions of any type i.e. line, corner or fan shaped can be easily implemented in the finite-volume method. A source term is included in the continuity equation for simulating the infiltration. The proposed model has been validated separately for surface flow and subsurface flow. Surface flow component has been validated using the data of Zhang and Cundy (1989) for two-dimensional surface flow considering effective rainfall. The subsurface flow component has been validated using the data of Hong et al. (1994). The present model has also been used to simulate the hypothetical urban catchment as shown in Fig.1. The runoff hydrograph before and after urbanization has been compared.

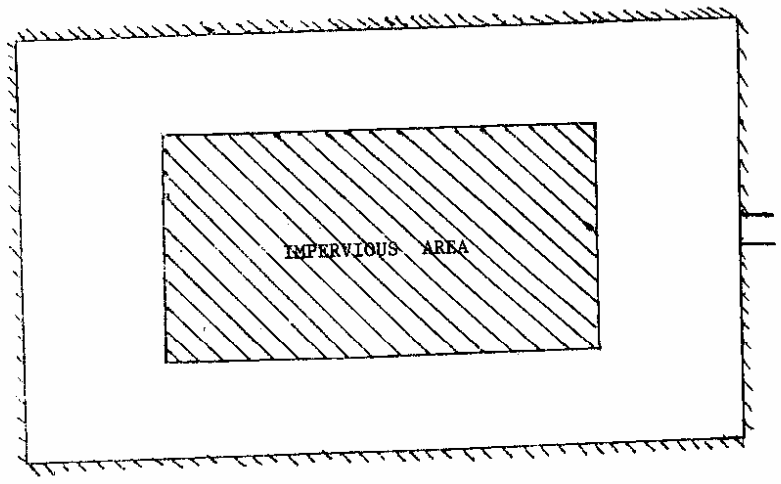

Fig. 1: Definition Sketch for the urban catchment with impervious area.

2. GOVERNING EQUATIONS

Mathematical modelling of overland flow for urban catchment involves solution of the governing equations for both the surface flow and subsurface flow with infiltration at the ground surface acts as the connecting link. In this study, the surface flow is represented by the two-dimensional shallow water flow equations with infiltration as a source term in the continuity equation while the subsurface flow is represented by the one-dimensional Richards equation in z-direction.

2.1 Surface Flow Equations

The surface flow is assumed to occur in a non-prismatic channel. The two-dimensional depth averaged shallow water flow equations which describe the laws of conservation of mass and momentum can be written as (Chaudhry 1993):

$$\frac{\partial U}{\partial t}+\frac{\partial E}{\partial x}+\frac{\partial G}{\partial y}= S \tag{1}$$

in which, U, E, G and S are vectors and are defined as

$$U = \begin{Bmatrix} h \\ uh \\ vh \end{Bmatrix}, \qquad E = \begin{Bmatrix} uh \\ u^2h+\frac{1}{2}gh^2 \\ uvh \end{Bmatrix}, \tag{2}$$

$$G = \begin{Bmatrix} vh \\ uvh \\ v^2h+\frac{1}{2}gh^2 \end{Bmatrix} \quad \text{and} \quad S = \begin{Bmatrix} (R-I) \\ gh(S_{ox}-S_{fx}) \\ gh(S_{oy}-S_{fy}) \end{Bmatrix} \tag{3}$$

where, h = flow depth; u = depth averaged velocity component along x dir.; v = depth averaged velocity component along y dir.; R = volumetric rate of rainfall per unit area; I = volumetric rate of infiltration per unit area; g = acceleration due to gravity; S_{ox} = catchment slope in x direction; S_{oy} = catchment slope in y direction; S_{fx} = friction slope in x direction; S_{fy} = friction slope in y direction. The derivation of the above

equations has been reported in Chaudhry, 1993 and is not repeated here. The assumptions in deriving the two-dimensional depth average shallow water flow equations are as follows:

1. The pressure distribution is hydrostatic. This is a valid assumption if the streamlines do not have sharp curvatures.

2. The channel bottom slope is small, so that the flow depths measured normal to the channel bottom and measured vertically are approximately the same.

3. The flow velocity along the depth is uniform.

4. The head losses in unsteady flow may be simulated by using the steady-state resistance laws, such as the Manning equation or Darcy-Weisbach equation.

Friction Slope

The friction slope is computed using the Darcy-Weisbach equation. Zhang and Cundy(1989) have differentiated between the resistance offered by the bed and the resistance due to the rainfall impact. They have used either the Manning equation or the Darcy-Weisbach equation to compute the resistance offered by the bed. They have developed a simple expression for the resistance due to the rainfall by assuming that the retardance effect of rainfall is predominantly caused by the momentum exchange between individual rain droplets and flowing water. The Darcy-Weisbach equation for computing the friction slope is given by

$$S_{fx} = \frac{f_d u\sqrt{u^2+v^2}}{8gh} \qquad S_{fy} = \frac{f_d v\sqrt{u^2+v^2}}{8gh} \tag{4}$$

where, f_d = frictional resistance coefficient. Evaluation of f_d depends on the instantaneous state of flow and is given by the following formulae.

(i) Laminar flow (Re < 900):

$$f_d = \frac{C_L}{Re} \tag{5a}$$

(ii) Transitional flow (900 < Re < 2000):

$$f_d = \frac{0.223}{Re^{0.25}} \tag{5b}$$

(iii) Fully turbulent flow (Re > 2000):

$$f_d = \left(2\log\frac{2h}{k}+1.74\right)^{-2} \tag{5c}$$

in which,

$$C_L = 24 + 0.21743\ R^{0.407} \tag{5d}$$

In the above equations, Re = Reynolds number = q/ν (ν = Kinematic viscosity of liquid), R = intensity of rainfall and k = a length measure of surface roughness.

2.2 Subsurface Flow Equations

The subsurface flow is considered as one-dimensional motion of a single-phase incompressible fluid. The one-dimensional, transient unsaturated flow equation in an isotropic porous medium is derived by applying the principle of conservation of mass and the basic Darcy's law for unsaturated flow and making the following assumptions.

(i) Compressibility of the medium and the water are negligible;
(ii) The air phase is stagnant and is at atmospheric pressure;

The one-dimensional continuity equation without source and sink within the flow domain can be written as

$$\frac{\partial\theta}{\partial t} + \frac{\partial V_z}{\partial Z} = 0 \tag{6}$$

where, θ = volumetric moisture content; V_z = Darcy flow velocity in the z direction; and z are distance along the coordinate direction. z is taken positive down wards. It is assumed that the Darcy's law is applicable for evaluating the velocity components. The Darcy's law for unsaturated flow in the z direction in an isotropic soil is

$$V_z = -K(\psi)\left(\frac{\partial \psi}{\partial z} - 1\right) \tag{7}$$

where, ψ =pressure head (m) and $K(\psi)$= unsaturated hydraulic conductivity (m/s) which depends on the pressure head, ψ. Substitution of Equation (7) in Equation (6) yields the Richards equation (Freeze and Cherry 1979):

$$\frac{\partial \theta}{\partial t} = \frac{\partial}{\partial z}\left[K(\psi)\left(\frac{\partial \psi}{\partial z} - 1\right)\right] \tag{8}$$

Equation is valid for transient subsurface flow in the unsaturated zone where the compressibility effects of the fluid and the medium are negligible. Equation is said to be in the "mixed form" of Richards Equation since it includes both the dependent variables θ and ψ. Most of the earlier studies on the overland flow have employed the Richards equation in either the pressure head form or the moisture content form. These equations are

Pressure Head form :

$$C(\psi)\frac{\partial \psi}{\partial t} = \frac{\partial}{\partial z}\left[K(\psi)\left(\frac{\partial \psi}{\partial z} - 1\right)\right] \tag{9}$$

Moisture content form :

$$\frac{\partial \theta}{\partial t} = \frac{\partial}{\partial z}\left[\frac{K(\psi)}{C(\psi)}\frac{\partial \theta}{\partial z} - K(\psi)\right] \tag{10}$$

in which, $C(\psi) = d\theta/d\psi$ = specific moisture capacity and $K(\psi)/C(\psi)$ = unsaturated diffusivity. Pressure head form of the Richards equation is applicable to the flows in saturated-unsaturated

zones and layered zones, but gives large mass balance errors. The moisture content form of the Richards equation perfectly conserves the mass within the flow domain, but is not applicable to the saturated flow zones and is also not applicable directly to the layered zones because of the discontinuities in moisture content profiles at the interfaces of layers. These difficulties are over come by using the mixed form of the Richards equation. It has been shown conclusively by Hills et al. (1989) and Celia et al. (1990) that the mixed form of the Richards equation result in better numerical behaviour than the other forms. It combines the benefits of both the pressure head and the moisture content forms of the Richards equations. Therefore, in the present study, Equations (6) and (7) are numerically solved to simulate the subsurface flow process.

The main difficulty in the Richards equation to actual field situations is the estimation of the parameters of the soil characteristic curves. Functional relationships are needed to the relationship between the hydraulic conductivity, the moisture content and the pressure head. In general, ψ-K and ψ-θ relationships are not unique and soils exhibit different behaviour during wetting and drying phases. This hysteresis is not considered here. However, the hysteresis can be included by employing different ψ-K and ψ-θ relations for wetting and drying processes. Several quasi-analytical equations are available to describe ψ-K and ψ-θ relations (Rawls and Brakensick, 1988). some very commonly used equations are given below.

Brooks-Corey (1964)

$$\frac{\theta-\theta_r}{\theta_s-\theta_r}=\left(\frac{\psi_b}{\psi}\right)^{\lambda_1} \quad \text{and} \quad \frac{K(\theta)}{K_s}=\left(\frac{\theta-\theta_r}{\theta_s-\theta_r}\right)^{3-\frac{2}{\lambda_1}} \tag{11}$$

Campbell (1974)

$$\frac{\theta}{\theta_s}=\left(\frac{H_b}{\psi}\right)^{\frac{1}{\lambda_2}} \quad \text{and} \quad \frac{K(\theta)}{K_s}=\left(\frac{\theta}{\theta_s}\right)^{2\lambda_2+3} \tag{12}$$

Van Genuchten (1980)

$$\frac{\theta-\theta_r}{\theta_s-\theta_r}=\left[\frac{1}{1+(\alpha\psi)^{\lambda_3}}\right]^{\lambda_4} \quad \text{and} \quad \frac{K(\theta)}{K_s}=\left(\frac{\theta-\theta_r}{\theta_s-\theta_r}\right)^{\frac{1}{2}}\left[1-\left\{1-\left(\frac{\theta-\theta_r}{\theta_s-\theta_r}\right)^{\frac{1}{\lambda_4}}\right\}^{\lambda_4}\right]^2 \quad (13)$$

where, $K(\theta)$ and θ are the hydraulic conductivity and the moisture content of the soil. K_s and θ_s are the saturated hydraulic conductivity and saturated moisture content. θ_r is the residual moisture content and ψ_b is the hypothetical bubbling pressure. λ_1, λ_2, λ_3 and λ_4 are constants.

The parameters of the soil moisture characteristic relationships should be specified a priori for field application of the Richards equation models. These values may be obtained from field observations using parameter estimation models. In this study, soil moisture characteristics derived from experimental and field data are employed.

3. NUMERICAL METHOD

The governing equations presented in the previous section are a set of non-linear partial differential equations for which analytical solutions are not available in idealized cases. Therefore, they are solved in the present study using numerical schemes.

3.1 Surface Flow

Surface flow equations constitute a set of nonlinear hyperbolic partial differential equations. These can be solved using the numerical methods. Many types of numerical methods such as finite-difference, finite-element and finite-volume methods are available for the solution of the hyperbolic partial differential equations. Finite-difference methods require approximations of the boundary if the domain is non-rectangular. They should have a grid with square corners, straight edges and

parallel lines. They can not easily simulate the natural boundaries but, they are very simple and easy to implement. On other hand, finite-element methods have an advantage over finite-difference methods in handling the irregular boundaries. However, they are computationally more intensive and are more difficult to implement than finite-difference schemes. Finite-volume methods are a viable alternative to the finite-element methods and are becoming popular these days. Finite-volume methods can easily handle non-rectangular domains and are as easy to implement as finite-difference methods. Therefore, in the present study, a finite-volume method is used for solving the governing equations. A recently developed high resolution finite-difference scheme (Nujic 1995) for the solution of dam break flows is converted into a finite-volume method by Singh, 1996. The main advantages of this scheme are its simplicity and ease of implementation. It can also handle sharp gradients in the water surface profile if they are present. The finite-volume scheme is an explicit scheme and is second order accurate in space and time. It is a two-step predictor-corrector scheme. A brief description of the scheme as applied in this study is presented below.

3.1.1 Finite-Volume Scheme

Figure 2 shows the finite-volume grid of the two-dimensional flow domain. The flow domain is divided into a set of cells (i,j), each of which is identified by the corresponding centre point. The finite-volume grid need not be orthogonal as in the case of a finite-difference grid. Figure 3 shows the non-orthogonal elemental cell (i,j) and its immediate neighbours.

The governing equations are integrated by a finite-volume technique on each of these cells covering the whole domain. Equation (1) can be written in an integral form as shown below after applying the Gauss divergence theorem.

$$\int_v \frac{\partial U}{\partial t} dv + \oint_s (\mathbf{F}.n)\, ds = \int S dv \qquad (14)$$

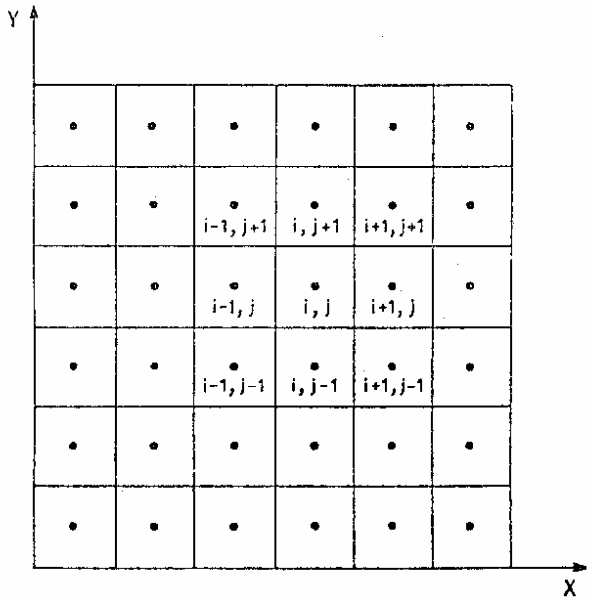

Fig. 2: Finite-volume grid for two-dimensional domain.

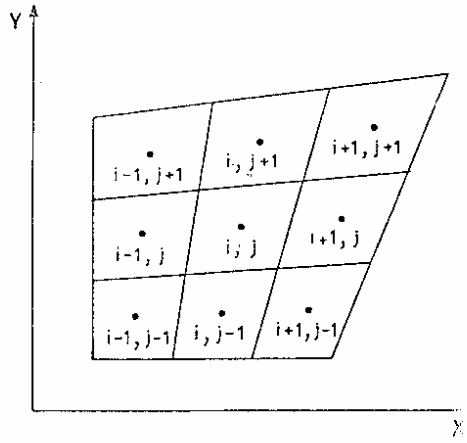

Fig. 3: Two-dimensional cells for any arbitrary shape of flow domain (Non-orthogonal cell).

where, F is the flux term at the control surface. The volume integral in the first term actually represents the integral of the time evolution of the function over the area of the cell. The surface integral in the second term is the total normal flux through the cell boundaries. The normal unit vectors to the cell walls are defined as shown in Fig. 4.

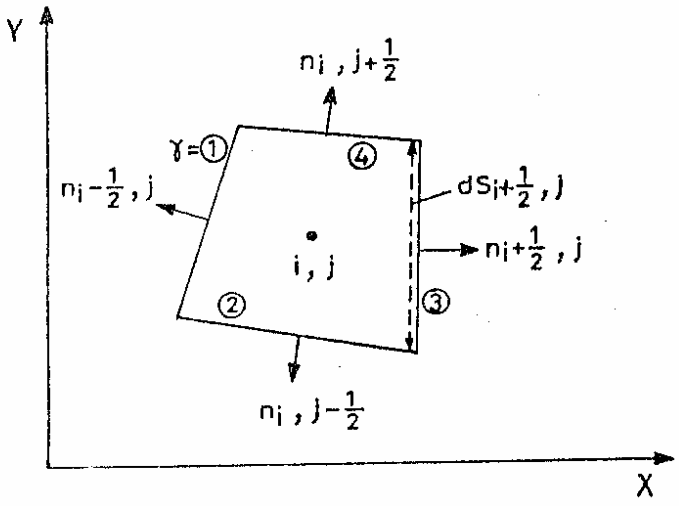

Fig. 4: Normal vectors at the cell faces in a cell of two-dimensional finite-volume grid.

The scalar product F.n in the second term of Eq. (14) can be expressed in terms of the Cartesian components as

$$F.n = En_x + Gn_y \tag{15}$$

where, n_x and n_y are the x and y components of the unit vector n. Assuming the vector U to be uniform over the cell, Eq. (14) can

be written as

$$\frac{\partial U}{\partial t}\Delta A+\oint_s (F.n)ds = S\Delta A \tag{16}$$

where, ΔA = area of the finite-volume cell. The surface integral in Eq. (16) is approximated by a sum over the four walls of the finite-volume in the following way.

$$\oint_s (F.n)ds \approx \sum_{r=1}^{4} (F_r.n_r)ds_r \tag{17}$$

where, ds_r = lengths of the four walls which contour the cell (i,j); F_r = the numerical flux through the cell faces r which contour the cell (i,j).

Evaluation of the numerical flux at a cell face is explained here for the cell face between the nodes (i+1,j) and (i,j). Similar procedure is adopted for other cell faces.

$$F_3.n_3=(F.n)_{i+\frac{1}{2},j}=\frac{1}{2}[F_R+F_L-\alpha(U_R-U_L)].n_{i+\frac{1}{2},j} \tag{18}$$

where, α = a positive coefficient, $F_R=f(U_R)$ = the flux computed using the information from the right side of the cell face and $F_L=f(U_L)$ = the flux computed using the information from the left side of the cell face. U_R and U_L are obtained using the following procedure.

$$(U_L)_{i+\frac{1}{2},j}=U_{i,j}+\frac{1}{2}\delta U_{i,j} \tag{19}$$

$$(U_R)_{i+\frac{1}{2},j}=U_{i+1,j}-\frac{1}{2}\delta U_{i+1,j} \tag{20}$$

where, the subscript (i,j) refers to the value at the node (i,j). The subscript (i+1/2,j) refers to the value at the interface between the nodes (i,j) and (i+1,j). There are several ways to determine $\delta U_{(i,j)}$ and $\delta U_{(i+1,j)}$ using different slope limiter procedures (Alcrudo et al. 1992). The "minmod" limiter is

followed in this study. According to this

$$\delta U_{i,j} = minmod\,(U_{i+1,j} - U_{i,j},\ U_{i,j} - U_{i-1,j}) \tag{21}$$

$$\delta U_{i,j} = minmod\,(U_{i+1,j} - U_{i,j},\ U_{i+2,j} - U_{i+1,j}) \tag{22}$$

where the minmod function is defined as

$$minmod = \begin{cases} a \ if\ |a| < |b| \ and\ ab > 0 \\ b \ if\ |b| < |a| \ and\ ab > 0 \\ 0 \ if\ ab \le 0 \end{cases} \tag{23}$$

The positive coefficient α is determined using the maximum value (for all the grid points) of the largest eigen value of the Jacobian of the Eq.(1). This is approximately given as

$$\alpha \ge \max\left|\left(V_{i,j} + \sqrt{g h_{i,j}}\right)\right| \qquad i = 1\ to\ N_i,\ j = 1\ to\ N_j \tag{24}$$

in which, N_i and N_j are the total number of grid points in the x and y directions, respectively, and $V_{i,j}$ is the resultant velocity. Integration of Eq.(16) in the time domain is done using a predictor-corrector approach as discussed below.

Predictor Part:

The predicted value of the vector U at the unknown time level t+Δt is determined using the following discretization of Eq.(16).

$$U^*_{i,j} = U^n_{i,j} - \frac{\Delta t}{\Delta A_{i,j}} \left[F^n_{i+\frac{1}{2},j}\, ds_{i+\frac{1}{2},j} + F^n_{i,j+\frac{1}{2}}\, ds_{i,j+\frac{1}{2}} + F^n_{i-\frac{1}{2},j}\, ds_{i-\frac{1}{2},j} + F^n_{i,j-\frac{1}{2}}\, ds_{i,j-\frac{1}{2}} \right] + \Delta t\, S^n_{i,j} \tag{25}$$

in which, the superscripts n and * refer to the value at the known time level, t and the predicted value at the unknown time level, t+Δt, respectively. Δt is the computational time step.

Equation (25) should be interpreted component wise for the vector U. Equation (25) gives the predicted values of h, u and v at the time level, t+Δt at any node (i,j).

Corrector Part:

The vector U at the corrector step ** and at the node (i,j) i.e. $U^{**}_{i,j}$ is computed using the predicted values and the values at the time level n.

$$U^{**}_{i,j} = U^{n}_{i,j} - \frac{\Delta t}{\Delta A_{i,j}} \left[F^{*}_{i+\frac{1}{2},j}\, ds_{i+\frac{1}{2},j} + F^{*}_{i,j+\frac{1}{2}}\, ds_{i,j+\frac{1}{2}} + F^{*}_{i-\frac{1}{2},j}\, ds_{i-\frac{1}{2},j} + F^{*}_{i,j-\frac{1}{2}}\, ds_{i,j-\frac{1}{2}} \right] + \Delta t\, S^{*}_{i,j} \quad (26)$$

Following the recommendations of Alcrudo et al. (1992), U^{*}_{R} and U^{*}_{L} (which are needed to compute F^{*} are determined from $U^{*}_{i+1,j}$ and $U^{*}_{i,j}$ using the same $\delta U_{i+1,j}$ and $\delta U_{i,j}$ which are already determined in the predictor step. This procedure results in better numerical stability.

$$(U^{*}_{L})_{i+\frac{1}{2},j} = U^{*}_{i,j} + \frac{1}{2}\delta U_{i,j} \quad (27)$$

$$(U^{*}_{R})_{i+\frac{1}{2},j} = U^{*}_{i+1,j} - \frac{1}{2}\delta U_{i+1,j} \quad (28)$$

Computation of F^{*} and S^{*} in Eq.(26) is similar to computation of F and S in Eq.(25) except that the predicted values of U are used instead of the values of U at the time level t.

The vector U at the unknown time level n+1 and at the node (i,j) i.e. $U^{n+1}{}_{i,j}$ is computed taking the average of the predicted values and the corrected values.

$$U^{n+1}_{i,j} = \frac{1}{2}\left(U^{*}_{i,j} + U^{**}_{i,j}\right) \quad (29)$$

3.1.2 Initial Conditions

Initial conditions are required at time t=0 to start the transient computations. At time t=0, the flow depth, the velocity components and the infiltration depth for all the cells are specified as the initial conditions. Although the initial flow depth is equal to zero, a very thin water film of depth h_{ini} is assumed to exist at time t=0. This assumption is made to overcome the numerical singularity in a simple way. It has been shown earlier (Singh and Bhallamudi, 1996) that such a procedure does not introduce significant errors. The velocity components and the infiltration depth are zero at all the cells at time t=0.

3.1.3 Boundary Conditions

The finite-volume grid is chosen such that the boundaries of the flow domain coincide with the cell faces of the control-volume cells. Boundary conditions are specified at all the outer cell faces of the flow domain. Two types of boundaries (i) flow boundary and (ii) no flow boundary are encountered in the overland flow model.

(i) *No flow boundary*: A schematic representation of a no flow boundary i.e. a solid wall boundary for the cell (i,j) is shown in Fig. 5a. Zero mass flux condition is specified as the boundary condition at the left face of the cell (i,j) while solving the continuity equation. This means

$$(uhn_x + vhn_y)_1 = 0 \tag{30}$$

Value of the flow depth at the face 1 is required for computating F at this face while solving the momentum equation.

In the present study, it is assumed that the flow depth at the face 1 is approximately equal to the flow depth at the centre of the cell. This means

$$(F.n)_{1\{x\text{-momentum}\}} \approx \frac{1}{2} g h_{i,j}^2 n_{x1} \tag{31a}$$

and

$$(F.n)_{1\{y\text{-momentum}\}} \approx \frac{1}{2} g h_{i,j}^2 n_{y1} \qquad (31b)$$

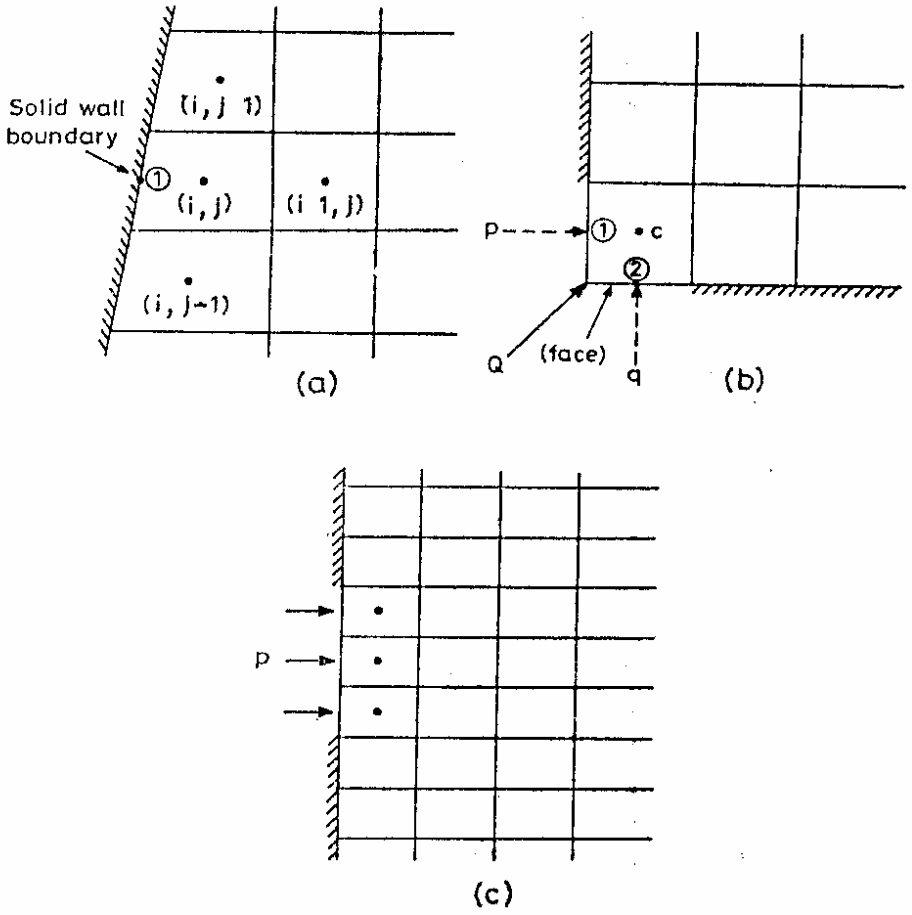

Fig. 5: Implementation of boundary conditions
(a) Solid wall (b) Corner Inflow and (c) Line Inflow.

(ii) *Flow boundary*: Flow boundaries are encountered for all those outer cells which receive the irrigation water from a source external to the domain. Two types of inflow boundary conditions are implemented in the proposed model. A description of each type follows.

Corner Inflow: Corner inflow corresponds to flooding of the domain from a point source located at a corner. As shown in Fig. 5(b), the total discharge assigned to the inflow, Q (m^3/s) is assumed to enter the cell from the faces 1 and 2 in equal amounts. Therefore, the unit discharges p and q (m^2/s) are computed as

$$p = \frac{Q}{2\Delta y}, \qquad q = \frac{Q}{2\Delta x} \tag{32}$$

The values of flow depth at the faces 1 and 2 are required to compute the flux at these faces while solving the momentum equations. Information from the centre of the cell can be used for this purpose only if the inflow is subcritical. Therefore, the flow depth at the face is computed as

$$h_{face} = Max(h_c, h_{critical}) \tag{33}$$

where, h_c=flow depth at the center of the cell and $h_{critical}$=flow depth computed from the critical flow considerations.

$$h_{critical} = 1.01\left(\frac{p^2+q^2}{g}\right)^{\frac{1}{3}} \tag{34}$$

It should be noted here that the critical depth is increased by 1% to ensure the subcritical flow conditions.

Line Inflow: Line inflow represents the flooding of domain from one face of one or more cells. Fig. 5(c) shows the line inflow from more than one cell. The total inflow, Q (m^3/s) is assumed to enter the cells from only one face. Therefore, the unit discharge

p (m^2/s) for each of the cells = $\frac{Q}{n_i \Delta y}$ in which n_i is the number of inflow cells. Procedure for calculating the flow depth at the cell face is similar to the procedure described for the corner inflow.

3.1.4 Numerical Stability

This finite-volume scheme is an explicit scheme and therefore, computational time step, Δt is dynamically computed at every time step using the following criterion (Alcrudo and Garcia-Navarro 1993).

$$\Delta t \leq \frac{\min\{dr(i,j)\}}{2\,Max\left\{\left(\sqrt{gh}+\sqrt{u^2+v^2}\right)_{i,j}\right\}} \qquad (35)$$

in which, dr(i,j) are the whole set of distances between every centre point (i,j) and those of its four adjacent cells.

3.2 Subsurface Flow

In order to determine the infiltration rate I in the continuity equation for the surface flow, the subsurface flow equations have to be solved along with an appropriate boundary condition at the ground surface. In the present study, a recently developed strongly implicit finite-difference scheme (Hong et al. 1994) for the mixed based formulation of the Richards equation is used to simulate the unsaturated subsurface flow conditions. This scheme ensures mass balance in its solution regardless of time step size and nodal spacings, and has no limitations when applied to field problems. It is also easy to incorporate different types of boundary conditions in this scheme. The subsurface flow is assumed to occur only in the vertical direction. In this study, the infiltration rate at any distance x is determined using the one-dimensional Richards equation with the surface flow depth at that point as the top boundary

condition. Numerical solution of the Richards equation is described in the following section.

3.2.1 Implicit Finite-Difference Scheme

The subsurface flow domain is divided into a number of rectangular blocks (Fig. 6a).

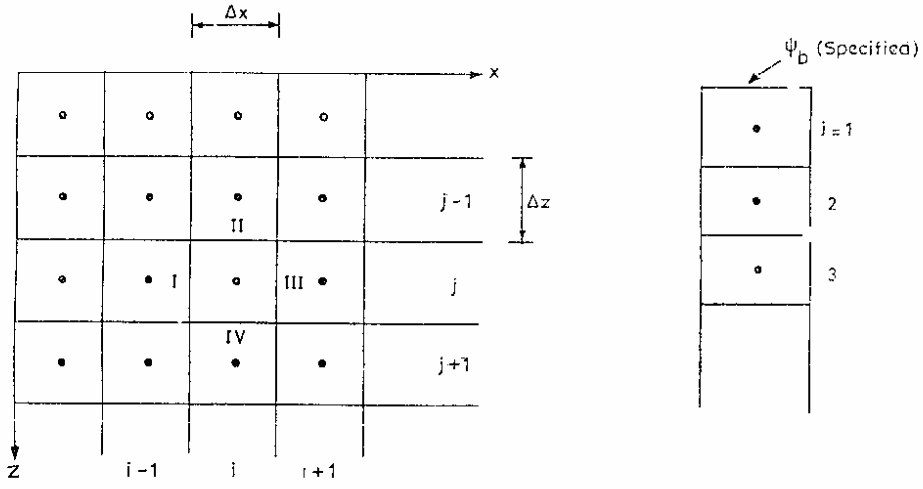

Fig. 6a: Finite-Difference Grid for Subsurface Flow.
6b: Definition Sketch of Pressure Head type Boundary for Subsurface Flow.

The moisture content, θ and the pressure head, ψ are specified at the centre of the block (the node), while the velocities are specified at the interblock faces. The subscript j refers to the block number in the z-direction. The superscripts n and n+1 refer to the known and the unknown time levels, respectively. The finite-difference form of the Eq. (6) is

$$\frac{\theta_j^{n+1} - \theta_j^n}{\Delta t} + \frac{\overline{V}_{IV} - \overline{V}_{II}}{\Delta Z} = 0 \qquad (36)$$

where, the bar is used to denote the time averaged value of the velocity. Δz is the nodal spacing in the z direction. The time-averaged velocities are determined by

$$\overline{V} = wV^{n+1} + (1-w)V^n \qquad (37)$$

in which, w=time weighting factor.

The velocity at any interblock face is determined using the pressure heads at the neighbouring cell centers. For example ;

$$V_{IV} = -\frac{K_{IV}\{(\psi_{j+1} - \psi_j) - \Delta z\}}{\Delta z} \qquad (38)$$

in which, K_{IV} is the unsaturated hydraulic conductivity evaluated at the interblock faces between the nodes (j+1) and (j). Substitution of Eqs. (37), and (38) in Eq. (36) yields

$$Res_j^{n+1} = \frac{w\Delta t}{\Delta z^2}\left[-K_{IV}^{n+1}\left(\psi_{j+1}^{n+1} - \psi_j^{n+1} - \Delta z\right) + K_{II}^{n+1}\left(\psi_j^{n+1} - \psi_{j-1}^{n+1} - \Delta z\right)\right] + \theta_j^{n+1} - \left[\theta_j^n - (1-w)\frac{\Delta t}{\Delta z}\left(V_{IV}^n - V_{II}^n\right)\right] = 0 \qquad (39)$$

The unsaturated hydraulic conductivity at an interblock face is estimated using the pressure heads at the neighbouring cell centers. Haverkamp and Vauclin (1979) state that the geometric mean is the best choice for estimating the interblock conductivities. However, Hong et al. (1994) reported that the iterative solution of Eq. (39) fails to converge if the above procedure s adopted for estimating the K. This is especially true for infiltration into initially very dry soils. The geometric mean is strongly weighted towards the lower value and therefore, water can not drain easily if the soil is initially dry. This results in a non-physical build up of pressure. In this study, the interblock hydraulic conductivity is estimated by the

weighted arithmetic mean. For example,

$$K_{IV} = \gamma K(\psi_j) + (1-\gamma) K(\psi_{j+1}) \tag{40}$$

in which, γ is the weight coefficient. Hong et al. (1994) suggest a value of 0.5 for γ.

Equation (39) is written for all the blocks in the flow domain and this results in a set of simultaneous algebraic equations in the unknowns $\psi(j)^{n+1}$. These simultaneous equations are highly non-linear since θ^{n+1} and K^{n+1} are non-linear functions of ψ^{n+1}. In the present study, they are solved by using the Newton-Raphson technique.

$$Res_j^{n+1,r} + \frac{\partial Res_j^{n+1,r}}{\partial \psi_m} \delta\psi_m = 0 \tag{41}$$

in which, r is the previous iteration level and $\delta\psi = (\psi^{n+1,r+1} - \psi^{n+1,r})$. Subscript m indicates the summation of the second term over all the blocks. Substituting of Eq. (39) in Eq. (41) yields a linear equation in $\delta\psi$ having the following form.

$$T_j^{n+1,r}\delta\psi_{j-1} + B_j^{n+1,r}\delta\psi_{j+1} + P_j^{n+1,r}\delta\psi_j + Res_j^{n+1,r} = 0 \tag{42}$$

in which, T, B, and P are the elements of the Jacobian of the system of equations, Eq. (39). Equations for evaluating these coefficients are as follows

$$T_j^{n+1,r} = \frac{w\Delta t}{\Delta z^2}\left[-K_{II}^{n+1,r} + \frac{D_j^{n+1,r}}{2}\left(\psi_j^{n+1,r} - \psi_{j-1}^{n+1,r} - \Delta z\right)\right] \tag{43}$$

$$B_j^{n+1,r} = \frac{w\Delta t}{\Delta z^2}\left[-K_{IV}^{n+1,r} - \frac{D_j^{n+1,r}}{2}\left(\psi_{j+1}^{n+1,r} - \psi_j^{n+1,r} - \Delta z\right)\right] \tag{44}$$

$$P_j^{n+1,r} = C_j^{n+1,r} + \frac{w\Delta t}{\Delta z^2}\left[-K_{IV}^{n+1,r} - \frac{D_j^{n+1,r}}{2}\left(\psi_{j+1}^{n+1,r} - \psi_j^{n+1,r} - \Delta z\right) + K_{II}^{n+1,r} + \frac{D_j^{n+1,r}}{2}\left(\psi_j^{n+1,r} - \psi_{j-1}^{n+1,r} - \Delta z\right)\right] \quad (45)$$

$$Res_j^{n+1,r} = \theta_j^{n+1,r} - \theta_j^n + \frac{w\Delta t}{\Delta z}\left(V_{IV}^{n+1,r} - V_{II}^{n+1,r}\right) + \frac{(1-w)\,\Delta t}{\Delta z}\left(V_{IV}^n - V_{II}^n\right) \quad (46)$$

Equation (42) when written for all the blocks in the domain constitutes a matrix equation

$$A^{n+1,r}\delta\psi = -Res^{n+1,r} \quad (47)$$

in which, the coefficient matrix A is tridiagonal. Equation (47) is solved in the present study using the standard subroutine for the solution of tridiagonal matrix.

For convergence in iteration of Eq. (41), it is required that

$$\left|Res_j^{n+1,r}\right| < \epsilon \quad (48)$$

in which, ϵ = water content convergence tolerance. Equation (48) practically represents the principle of mass conservation because usually a very small value of ϵ in imposed.

3.2.2 Boundary Conditions

(i) *Flux-Type Boundary Conditions*: In the adopted scheme, the grid is arranged in such a manner that the boundaries of the flow domain coincide with an interblock. Therefore, flux or velocity-type boundary condition can be incorporated in a natural

way in Eq. (36).

(ii) *Pressure Head-Type Boundary condition*: Referring to Fig. 6(b), let ψ_b be the imposed pressure head at the ground surface of the flow domain. This pressure head ψ_b is used along with the values of ψ_1 and ψ_2 to determine the flux at the ground surface as given below.

$$V_z\Big|_{z=0} = -K(\psi_b)\left[\frac{\left(-\frac{8\psi_b}{3}+3\psi_1-\frac{\psi_2}{3}\right)}{\Delta z}-1\right] \tag{49}$$

Second-order forward finite-difference analog is used to determine the above Eq. (49). Equation 39 and equations for the coefficients T, B & P are appropriately changed to include the boundary conditions before the matrix $A^{n+1,r}$ in Eq. (47) is formed.

3.3 Surface and Subsurface Flow Interaction

Surface and subsurface flow components are interrelated by a common pressure head and the infiltration at the ground surface. The top boundary condition for the subsurface flow is determined by the surface flow depth. In turn, the infiltration term in the surface flow equation is controlled by the subsurface flow conditions. The following procedure is adopted for simulating the interaction between the surface and the subsurface flow components.

1. Subsurface flow solution at time level n is used to determine the infiltration rate at the ground surface.

2. Surface flow equations are now solved using the infiltration rate from step 1 to determine q and h at the unknown time level n+1.

3. The surface flow depth at the time level n+1 is used as the top boundary condition and the subsurface flow equations

are solved. This gives the θ and ψ distribution in the subsurface at time level n+1.

4. Steps 1-3 are repeated up to the required time level.

As mentioned earlier, above is a decoupled approach which reduces the CPU time by half without significantly affecting the accuracy of the results.

Boundary Conditions:

For subsurface flow resulting from rainfall infiltration, the top boundary condition changes with time. During the initial stages of the rainfall, there is no ponding and the infiltration rate is equal to the rainfall rate. The top boundary condition for such a situation is the specification of the flux equal to the rainfall rate. As time progresses, the upper layers of the subsoil get saturated and then infiltration rate starts decreasing. Before starting the solution of the Richards equation for any time step, the flux at the top boundary is estimated by taking $\psi_b = 0$. If this velocity is greater than the rainfall rate, then the flux type of boundary condition is applied. Otherwise, a head type of boundary condition ($\psi_b(x) = h(x) =$ water flow depth at that point) is applied. The time to ponding comes out as a part of the solution.

A no flux boundary condition is imposed at the right and left boundaries. The ψ values at the bottom boundary are obtained using a simple extrapolation from the interior points. This approximation does not introduce errors because the bottom boundary is taken fairly deep and the moisture front does not reach their for the computational times considered.

4. RESULTS AND DISCUSSION

4.1 Validation of the Model

In order to verify the present model, first the surface and subsurface flow components are tested separately with available experimental data and analytical solutions. Then, both the components have been linked together. A hypothetical urban catchment has been simulated using the present model.

4.1.1 Surface Flow

First of all the two-dimensional surface flow model was tested with the results of Zhang and Cundy (1989) for overland flow on a rectangular domain with spatial variation of surface roughness. Zhang and Cundy (1989) conducted the simulation with a rainfall of 15 cm/hr and infiltration rate of 5 cm/hr. Infiltration was continued after the end of rainfall at 3.5 minutes. The rectangular domain was 12 m long and 12 m wide with a 5 % gradient tilting in the x-direction. A differentiation was made between the resistance to the flow due to the bottom roughness and due to the rainfall impact. Effective friction slopes in x and y directions were computed using the following equations (Zhang and Cundy 1989):

$$S_{fx} = \frac{Ru}{gh} + \frac{f_d u\sqrt{u^2+v^2}}{8gh} \quad \text{and} \quad S_{fy} = \frac{Rv}{gh} + \frac{f_d v\sqrt{u^2+v^2}}{8gh} \tag{50}$$

where, f_d = frictional resistance coefficient and is given by:

$$f_d = \frac{\kappa_o \nu}{h\sqrt{u^2+v^2}} \tag{51}$$

The resistance parameter, κ_o was used to represent the surface roughness and assumed to vary according to a lognormal probability density function. Zhang and Cundy (1989) generated the κ_o values randomly from a lognormal function with a mean of 512 and standard deviation of 154. The values of κ_o assigned to

each of the finite-volume grids on the plane are given in Table-1 (Reproduced from Zhang and Cundy, 1989). The above test case was simulated using the present model with a grid size of $\Delta x = \Delta y = 1.0$ m. Initial flow depth on the plane, h_{ini} was equal to 1.0×10^{-4} m and Courant number, C_n was equal to 0.8.

Table 1: Spatial Distribution of Surface Roughness

j/i	1	2	3	4	5	6	7	8	9	10	11
1	295	288	312	650	698	287	486	710	460	744	538
2	472	591	603	450	276	529	585	405	418	543	332
3	631	404	728	494	616	510	648	752	412	744	264
4	521	385	458	426	599	345	677	775	262	556	647
5	557	723	372	690	634	593	271	466	396	286	358
6	701	256	692	761	458	373	248	531	468	361	498
7	710	272	721	402	688	549	561	502	759	570	755
8	533	313	678	275	457	388	521	284	264	826	497
9	451	414	691	612	732	498	663	298	526	570	366
10	491	653	627	584	727	481	266	748	699	440	298
11	405	639	650	578	357	450	340	663	447	252	545

The outflow hydrograph for a uniform κ_o value equal to 512 obtained using the present model is compared with the numerical results of Zhang and Cundy (1989) in Fig. 7. It can be clearly seen that the present model essentially gives the same results as simulated by Zhang and Cundy (1989). The difference in the results towards the end of the simulation could be due to different downstream boundary conditions adopted in the simulations. Extrapolation procedure was adopted in the present study while a critical flow condition was implemented by Zhang and Cundy (1989). It should be noted here that the simulations by Zhang and Cundy (1989) used a C_n value of 0.08 which means the present model is 10 times computationally faster than their model.

Figure 8 shows the comparison of numerical results for the outflow hydrograph, obtained using the variable roughness

surface. Although the hydrograph peaks simulated using the present model and by Zhang and Cundy (1989) match satisfactorily, the present model does not show any oscillations.

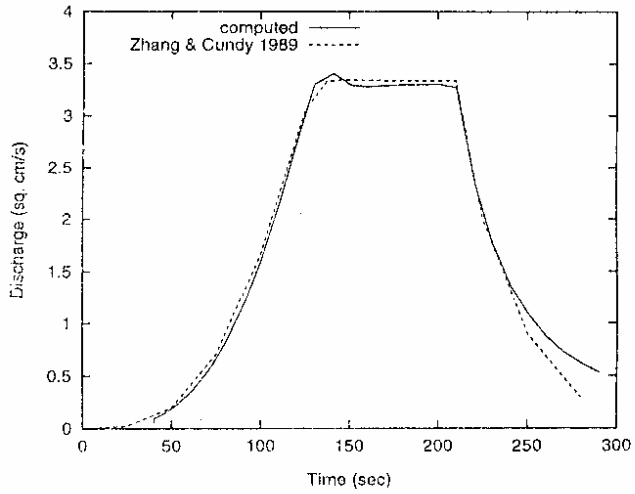

Fig. 7: Comparison of outflow hydrograph from surface flow model with uniform surface roughness.

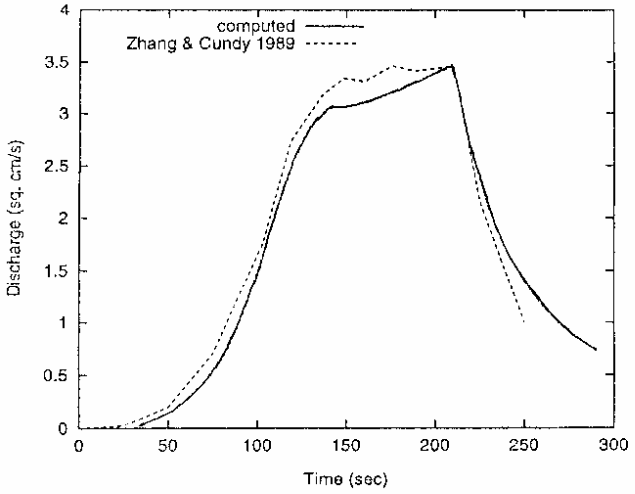

Fig. 8: Comparison of outflow hydrograph from surface flow model with variable surface roughness.

4.1.2 Subsurface Flow

In order to verify the subsurface flow component of the present model, a problem of one-dimensional infiltration into a uniform sand column, for which a analytical solution by Philip and Haverkamp is available. In this problem, the computational parameters are taken as given below in Table-2.

Table 2: Computational parameters for Subsurface flow

$$K = K_s \frac{A}{A+|\psi|^m}, \qquad \theta = \theta_r + \frac{B(\theta_s - \theta_r)}{B+|\psi|^n}$$

$K_s = 34\,cm/hr, \quad A = 1.175\times10^6, \quad m = 4.74,$

$\theta_s = 0.287, \ \theta_r = 0.075, \ B = 1.611\times10^6, \ n = 3.96,$

$\theta(z, t=0) = 0.1, \quad \psi(0\,cm, t>0) = -20.73\,cm,$

$\Delta z = 1\,cm, \quad \epsilon = 1\times10^{-5}, \ and \ \ w = 1$

The lower boundary condition has been considered as free drainage and upper boundary condition has been considered as the specified pressure head boundary.

The calculated moisture content profiles at times t = 0.1, 0.2 and 0.8 hours are presented in Fig. 9 along with the analytical values of Haverkamp and Vauclin (1979). The figure shows the good agreement with the earlier numerical results. The infiltration rate and cumulative infiltration per unit area obtained by present model and Haverkamp and Vauclin (1979) are presented in Figs. 10 and 11. Again figure shows the good agreement between these two results.

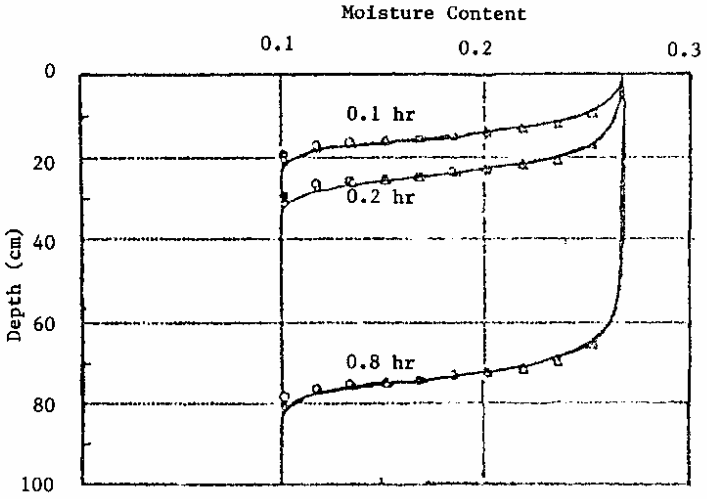

Fig. 9: Comparison of moisture content profile for subsurface flow model.

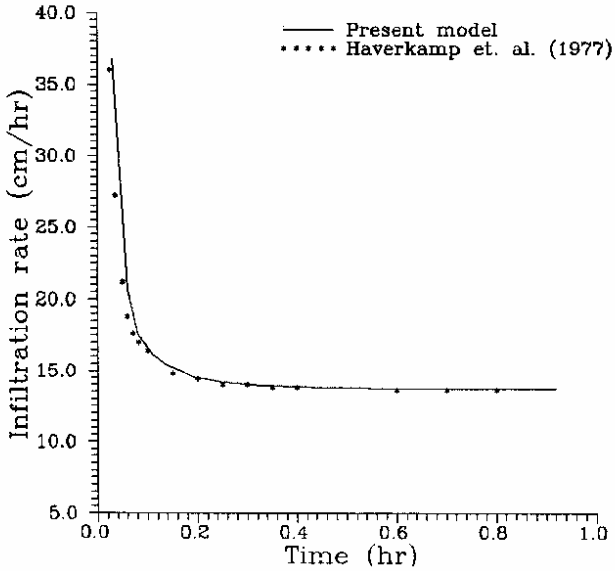

Fig. 10: Comparison of Infiltration rate with earlier results.

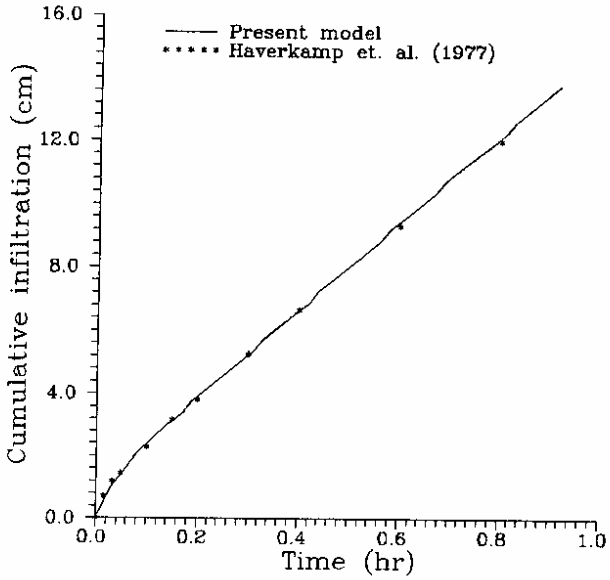

Fig. 11: Comparison of Cumulative Infiltration with earlier results.

4.2 Simulation of Hypothetical Urban Catchment

Numerical simulation was carried out using present model to demonstrate the applicability. For this purpose, a hypothetical urban catchment (Fig. 1) has been considered having length = 16 m., width = 16 m., longitudinal slope of 0.05 in x-direction only. The viscosity of the fluid, ν = 1.94 X 10^{-4} m^2/s. The rainfall intensity was considered 250 mm/hr over a duration of 10 minutes. The model has been run for a duration of 12 minutes. The hydraulic properties of the soil were taken from Singh (1996). The relative hydraulic conductivity, K_r and the effective saturation, S_e are defined as

$$K_r = \frac{K}{K_s}, \quad \text{and} \quad S_e = \frac{(\theta - \theta_r)}{(\theta_s - \theta_r)} \tag{52}$$

in which, K_s and θ_s are the saturated hydraulic conductivity and saturated moisture content, θ_r is the residual moisture content. The curve for S_e vs pressure head and K_r vs pressure head are represented in the present study using the following equations.

$$S_e = \begin{cases} \left(\frac{\psi_b}{\psi}\right)^{\lambda} & if\ \psi \le -12.85\,cm \\ 0.8434 - 0.0148\psi - 0.0026\psi^2 & if\ -12.85 \le \psi \le -2.8\,cm \\ 0.8642 & if\ \psi > -2.8\,cm \end{cases} \tag{53}$$

$$K_r = \begin{cases} \left(\frac{\psi_b}{\psi}\right)^{\eta} & if\ \psi \le -13.729\,cm \\ 0.5228 + 0.0204\psi - 0.0009\psi^2 & if\ -13.729 \le \psi \le -1.0\,cm \\ 0.5015 & if\ \psi > -1.0\,cm \end{cases} \tag{54}$$

The values of K_s, θ_s, θ_r, λ, η and ψ_b (hypothetical bubbling pressure potential) for the soil are given in Table 3.

Table 3: Hydraulic Properties of the Soil

K_s (cm/day)	θ_s	θ_r	λ	η	ψ_b (cm)
566.9	0.46	0.02	2.03	8.09	-10.0

The finite-volume grid spacing in the x and y directions, Δx and Δy were equal to 1.0 m and 1.0 m respectively and grid spacing in z direction was 2.74 cm, and Courant number, C_n = 0.65. A very small value of initial flow depth of 0.2 mm was taken to overcome the singularities problem. The numerical parameters for subsurface flow computations were: w = 1.0, and $\epsilon = 10^{-3}$.

In this model, the infiltration rate has been calculated at a point in the flow domain and used for all grid of the catchment having uniform soil type, assuming uniform infiltration rate all over the catchment. Since the whole catchment surface is ponded at the same time and the wetting front moves essentially in the vertical direction, the assumption of uniform infiltration rate all over the catchment is valid if the soil parameters are same and surface flow depth does not have a significant effect on the infiltration rate (Singh, 1996). The above assumption significantly reduce the computational time and computes the exact value of the infiltration rate based on soil physical parameters.

Figure 12 shows the runoff hydrograph at the downstream end (x=14 m) for three different percentage of catchment imperviousness (i.e. 0 % impervious means without any impervious area, 50 % means 50 % of the catchment area was impervious at the centre of the catchment and 100 % means whole catchment area was impervious) for the above numerical experiment.

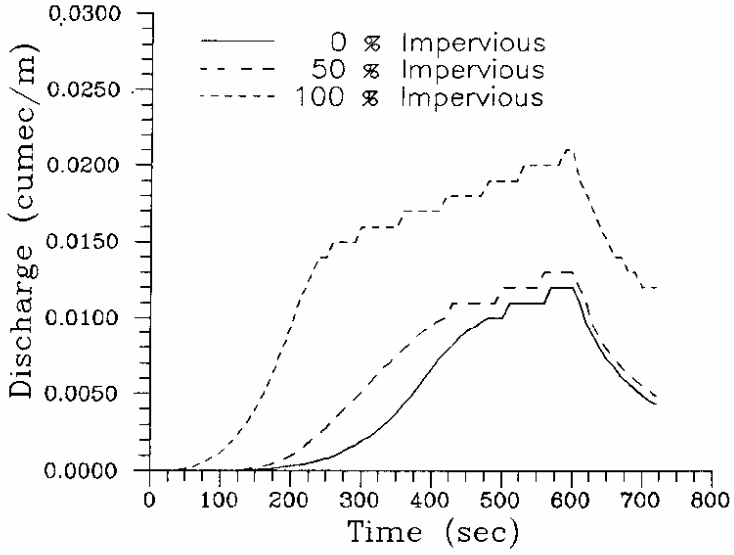

Fig. 12: Effect of urbanization on runoff hydrograph.

It can be seen from figure that as the imperviousness increases the runoff increases. The runoff hydrograph for 50 % impervious Curve does not shows that much increment as the 100 % impervious curve shows, because the impervious area has been considered in the centre of the catchment and there is a pervious area after the impervious area, so some water infiltrates into the ground. At the end of the rainfall there is a increase in runoff hydrograph in the 100 % impervious, this is due to the impact of the rainfall on the friction factor.

5. CONCLUSION

In this study, a two-dimensional surface flow model has been developed along with the one-dimensional subsurface flow model for infiltration, for simulation of the overland flow in urban catchment. In this model, the complete two-dimensional Saint-Venant equations have been solved using a simple, explicit finite-volume scheme. The subsurface flow component in the present model is represented by one-dimensional Richards equation in the mixed form. This equation has been solved by a recently developed strongly implicit finite-difference scheme. The proposed model does not require the approximation of boundaries by a stair-case type of grid in case of irregular field shapes. The depth and the discharge calculations are not staggered and iterations are not required for the velocity computations. Therefore, it is computationally more efficient than other finite-difference schemes.

The model has been validated separately for surface and subsurface flow components. Surface flow component is validated using the numerical results of Zhang and Cundy (1989). Here the two-dimensional surface flow has been used to simulate the randomly varying surface roughness. The subsurface flow component has been validated using the results of Hongs et al. (1994). The present model has also been used to simulate the hypothetical urban catchment with impervious area inside the catchment. The effect of imperviousness i.e. extent of urbanization, on the

runoff hydrograph has been presented. In this model, the uniform infiltration rate has been assumed all over the catchment, which have same physical soil parameters. This assumption save the computational time and compute the exact value of the infiltration which is used for the solution of the surface flow equations for surface runoff. This model can be used for the exact computation of the surface runoff from the urban catchment considering the soil moisture characteristic of that catchment.

Future Scopes and Suggestions are: This model should be applied to the real urban catchment considering the soil moisture characteristic of that catchment. Routing Subroutine should be added to this programm so that the runoff hydrograph can be calculated at any point of the outlet drainage ditches. Another Subroutine for networking of the drainage system should also be added and design of the suitable drainage system should also be added to this code.

REFERENCES

1. Alcrudo F., Garcia - Navarro P., and Saviron, J.M., 1992, "Flux difference splitting for 1D open channel flow equations", *Int. J. numerical methods in fluids*, 14, 1009-1018.

2. Alcrudo, F., and Garcia-Navarro, P., 1993,"A High-Resolution Godunov Type Scheme in Finite Volumes for the 2D Shallow Water Equations", *International Journal for Numerical Methods in Fluids*, 16, 489 - 505.

3. Celia, M.A., Bouloutas, E.F., and Zarba, R.L., 1990,"A general mass-conservative numerical solution for the unsaturated flow equation", *Water Resources Research*, 26(7), (1990), 1483-1496.

4. Chakraborti, A. K., 1989, "Urban Storm Water runoff modelling-A case study in Rohini Delhi", *WRD IIRS*, Dehradun, Report.

5. Chaudhry, M.H., *Open-channel flow*, Prentice-Hall, Englewood Cliffs, New Jersey, 1993.

6. Davis, K., 1965, "The Urbanization of the Human Population", *Scientific Am.*, 213(3), 40-54.

7. Freeze, R.A. and Cherry, J.A., 1979, *Ground Water*, Prentice-Hall, Englewood Cliffs, New Jersey.

8. Haverkamp, R., and Vauclin, M., 1979, "A note on estimating finite-difference interblock hydraulic conductivity values for transient unsaturated flow problems", *Water Resources Research*, 15(1), 181-187.

9. Hills, R.G., Porro, I., Hudson, D.B., and Wierenga, P.J., 1989, "Modeling one-dimensional infiltration into very dry soils,1. Model development and evaluation", *Water Resources Research*, 25(6), (1989), 1259-1269.

10. Hong, L. D., Akiyama, J., and Ura M., 1994, "Efficient mass-conservative numerical solution for the two-dimensional unsaturated flow equation", *J. of Hydroscience and Hydraulic Engineering*, 11(2), 1-18.

11. Lazaro, T. R., 1990, "*Urban Hydrology,*" Technomic Publishing Co. Inc., Lancaster.

12. McPherson, M. B., 1974, "Hydrological effects of urbanisation, *UNESCO PRESS*, Paris.

13. Nujic, M., 1995, "Efficient implementation of non-oscillatory schemes for the computation of free-surface flows", *J. Hydraulic Research*, IAHR, 33(1), (1995), 101-111.

14. Ramaseshan, S., 1983, "Progress since 1979 in India", Section II", *International Symposium on Urban Hydrology*, ed. by J. W. Delleur and H. C. Torno, Urban Water Resources Research Programme, ASCE, New York.

15. Raws, W. J., and Brakensiek, D. L., 1988, "Estimation of Soil Hydraulic Properties", *J. Morel-Seytoux (ed)*, unsaturated Flow in Hydrologic modelling, Riedel, 275--300.

16. Savini, J. and Kammerer, J. C., 1961, "Urban Growth and the Water Regimen," *US Geological Survey Water Supply*, Paper No. 1591-A, 43.

17. Singh, V., 1996, "Computation of Shallow Water Flow Over a Porous Medium", *Ph D Thesis*, Civil Engg. Department, I. I. T. Kanpur, India.

18. Singh, V., Bhallamudi, S. M., 1996, "Complete hydrodynamic border-strip irrigation model", *J. of Irrig. and Drain. Engrg.*, ASCE, 122(4), 189-197.

19. UNESCO, 1978, *"Research on Urban hydrology"*, Vol. I and II.

20. Zhang, W., and Cundy, T. W., 1989, "Modeling of two-dimensional overland flow", *Water Resources Research*, 25(9), (1989), 2019-2035.

APPENDIX I. Notation

C_n : Courant number;
c : wave speed;
ds_r : lengths of the four walls which contour the cell (i,j);
F_r : numerical flux through the cell face r which contour the cell (i,j);
f_d : frictional resistance coefficient;
g : acceleration due to gravity (m/s^2);
h : flow depth (m);
h_{ini} : depth of flow for the initial condition
I : volumetric rate of infiltration per unit area (m/s);
iflag, jflag :represents wave front location in x and y irection respectively
$K(\psi)$: unsaturated hydraulic conductivity (m/s);
k : length measure of surface roughness;
n : Manning roughness coefficient
n_x & n_y : unit vectors in x and y directions respectively.
N : total number of grid points in x direction;
Q : total discharge (cumec)
q : discharge per unit width (m^2/s);
q_{ini} : discharge specified as the initial condition;
R : volumetric rate of rainfall per unit surface area (m/s);
Re : eynolds number = q/v;
S_{ox} & S_{oy} : bottom slope in x and y directions respectively;
S_{fx} & S_{fy} : friction slope in x and y directions respectively;
t : time (sec);
U, E, G & S : vectors;
V : resultant velocity (m/s);
V_x : Darcy flow velocity in the x direction;
V_z : Darcy flow velocity in the z direction;
u & v :depth averaged velocity components in x and y directions respectively;
x & z: distances along the two coordinate directions;
α : a positive coefficient;
ΔA : area of the finite-volume cell (m^2);
Δt : time stepping;
ν : Kinematic viscosity of liquid;
ψ : pressure head (m);

ψ_b : imposed pressure head at the ground surface;
ψ_1 : pressure head at first grid under the ground;
ψ_2 : pressure head at second grid under the ground;
θ : volumetric moisture content.

Superscripts

n,*,** : refers to the values of the variables at known time level, the predicted and the corrected values;

Subscripts

i : refer to the grid point in x-direction;
j : refer to the grid point in y-direction;
r : denotes the walls

Director:	Dr. S. M. Seth	
Divisional Head:	Dr. G. C. Mishra,	Sc 'F'
Study Group:	Dr. Vivekanand Singh,	Sc 'B'